

SIMULATION OF OPTICAL MEDIA MOLDING

Bingfeng Fan¹ and David Kazmer²

¹*Dept. of Mech. & Ind. Engr., University of Massachusetts Amherst, Amherst, MA 01003*

²*Department of Plastics Engineering University of Massachusetts Lowell, Lowell, MA 01854*

Abstract

A hybrid finite element/finite difference method is employed to solve the temperature and pressure fields of an injection-compression molding process using a non-isothermal compressible flow model. The process simulation is coupled with a thermal viscoelastic material model to predict residual stress, warpage, and birefringence. A finite element analysis is formulated using axisymmetric plate elements to simulate the thermal stress and warpage. Flow and thermally induced birefringence is calculated by applying the stress-optical rule to the predicted residual stress. Experimental validation of injection-compression molded CD-R substrates shows that the simulation well predicts the process and part qualities under various processing conditions.

Introduction

Injection-compression molding is widely used in manufacturing of high capacity storage optical media, such as compact discs (CDs) and digital video discs (DVDs), using optical grade polycarbonate. This paper is focused on the process and quality simulation of a coining type of injection-compression molding. In this process, the thickness of the mold cavity is set to be slightly less than the nominal thickness of the part initially. During both the filling and packing stages, a balance is always maintained between the force exerted by the cavity pressure and the clamp tonnage. Depending on the growth and decline of the two forces, the mold halves may be blown open or closed. This continuous mold opening and closing, often referred to as "mold breathing", is distinctive from injection molding, and improves the mold filling and the replication of grooves or pits at the surface of the discs, as well as reduces the packing pressure, residual stress, and birefringence in the part.

The residual stress in the molded parts is a critical quality, since it causes warpage and birefringence, which greatly reduces the dimensional stability and the signal to noise ratio in the player. It is desirable to develop a computer simulation of the coining process that predicts the residual stress, warpage and birefringence. Such a simulation can not only provide vital insights into various causes of the mechanical and optical properties, but also provide valuable assistance in material and process

development to reduce the warpage and birefringence during mass production.

Process Simulation

The numerical methods originated by Chiang et al [1] for the simulation of injection molding are extended to the injection-compression molding. The modeling of the flow in the sprue follows directly from Chiang et al [1]. The disc is treated as one-dimensional geometry, and the disc elements are formulated as strips with incremental width so that the governing equations for channel flow can be used for modeling disc geometries, which compares well to the formulation in cylindrical coordinates for an element length on the order of the thickness. The continuity, momentum, and energy equations are:

$$\frac{\partial \rho}{\partial t} + \frac{\partial}{\partial x}(\rho u) + \frac{\partial}{\partial z}(\rho w) = 0 \quad (1)$$

$$\frac{\partial}{\partial z} \left(\eta \frac{\partial u}{\partial z} \right) = \frac{\partial P}{\partial x} \quad (2)$$

$$\rho C_p \left(\frac{\partial T}{\partial t} + u \frac{\partial T}{\partial x} \right) = \frac{\partial}{\partial z} \left(k \frac{\partial T}{\partial z} \right) + \eta \dot{\gamma}^2 \quad (3)$$

where ρ is density, x and z , u and w are the flow and gapwise directions and velocities, η is the viscosity, P is the pressure, T is the temperature, $\dot{\gamma}$ is the shear rate, C_p and k are the specific heat and thermal conductivity of the polymer respectively.

The boundary conditions are:

$$u = 0 \text{ at } z = \{0, h\}, \text{ and } T = T_w|_{z=0,h}$$

Integrating Eq 2 twice over the gapwise direction with the aid of the boundary condition and substituting the resultant velocity into Eq 1 yields:

$$\frac{\partial}{\partial x} \left(\tilde{S} \frac{\partial P}{\partial x} \right) = G \frac{\partial P}{\partial t} + F + \rho_h \dot{h} \quad (4)$$

where $\tilde{S} = \int_0^h \left(\rho \int_z^h \frac{(\tilde{z} - \lambda)}{\eta} d\tilde{z} \right) dz$ with $\lambda = \int_0^h \frac{z dz}{\eta} / \int_0^h \frac{dz}{\eta}$,

$G = \int_0^h \left(\frac{\partial \rho}{\partial P} \right)_T dz$, $F = \int_0^h \left(\frac{\partial \rho}{\partial T} \right)_P \frac{\partial T}{\partial t} dz$, $\dot{h} = dh/dt$ is the mold closing or opening speed, and ρ_h is the density of the polymer at the moving mold wall.

Galerkin's method is employed to solve Eq 4 to obtain the pressure field. The temperature field is obtained by solving the energy equation using a finite difference method.

Warpage Prediction

The thermal stress is modeled following the methodology originated by F. P. T. Baaijens [2]:

$$\boldsymbol{\sigma} = -p^h \mathbf{I} + \boldsymbol{\sigma}^d \quad (5)$$

$$p^h = -\frac{1}{3} \text{tr}(\boldsymbol{\sigma}) = \int_0^t \left(\frac{\alpha}{\kappa} \dot{T} - \frac{1}{\kappa} \text{tr}(\dot{\boldsymbol{\varepsilon}}) \right) d\tau$$

$$\boldsymbol{\sigma}^d = \sum_{i=1}^m 2 \int_0^t g_i e^{-(\xi(t)-\xi(\tau))/\theta_i} \dot{\boldsymbol{\varepsilon}}^d d\tau$$

where $\boldsymbol{\sigma}^d$, and $\dot{\boldsymbol{\varepsilon}}^d$ are the deviatoric stress and strain rate tensors; g_i and θ_i are the shear moduli and the corresponding relaxation times which are determined by dynamic mechanical measurement, and m is the number of modes; T is the temperature; p^h is the hydrostatic pressure and \mathbf{I} is the unit tensor. The temperature dependent thermal volume expansion coefficient, α , and the isothermal compressibility coefficient, κ , in the expression of hydrostatic pressure are defined as $\alpha = \frac{1}{v} \left(\frac{\partial v}{\partial T} \right)_p$,

$\kappa = -\frac{1}{v} \left(\frac{\partial v}{\partial P} \right)_T$, and $\xi(t)$ is the pseudo time defined by

$$\xi(\tau) = \int_0^\tau \frac{1}{a_T(T)} ds, \text{ where } a_T \text{ is the time temperature shift factor.}$$

After demolding, the thermal stress and warpage of the disc are modeled by a finite element analysis (FEA) to estimate the post-molding deformation. The elements chosen are 2-noded 1-D axisymmetric thin plate elements discretized along the radial direction. Each node has 3 degrees of freedom:

$$\mathbf{D} = [u \quad w \quad \phi]^T$$

corresponding to radial and vertical displacement as well as rotation to consider both in-plane and out of plane displacements [3]. The main assumptions of the finite element analysis are:

1. Based on the classical Kirchhoff thin plate theory, there is no transverse shear deformation.
2. $u(r, z) = \bar{u}(r) - z\bar{\varphi}(r)$, where $\bar{\varphi}(r) = \frac{d\bar{w}(r)}{dr}$ is the rotation, $\bar{u}(r)$ and $\bar{w}(r)$ are the radial and vertical displacements of the mid-plane of the disc.
3. $w(r) = \bar{w}(r)$, which means the vertical displacement does not vary through the thickness.

The set of linear equations to be solved can be written as:

$$\mathbf{K}\Delta\mathbf{D} = \mathbf{R} \quad (6)$$

where \mathbf{K} is the global stiffness matrix, $\Delta\mathbf{D}$ is the displacement increment vector to be solved, and \mathbf{R} is the right-hand side vector.

The element stiffness matrices can be written as:

$$\mathbf{k}^e = \int_V \mathbf{B}^T \mathbf{H} \mathbf{B} dV = 2\pi \int_{-h/2}^{h/2} \int_{r_1}^{r_2} \mathbf{B}^T \mathbf{H} \mathbf{B} r dr dz$$

where \mathbf{B} is the strain-displacement vector defined in the strain-displacement relationship $\Delta\boldsymbol{\varepsilon} = \sum_{i=1}^2 \mathbf{B}_i \Delta\bar{u}_i$, \mathbf{H} is the rigidity matrix defined in stress-strain relationship $\boldsymbol{\sigma} = \mathbf{H}\Delta\boldsymbol{\varepsilon} + \mathbf{h}$ to be determined by the viscoelastic relaxation data, and \mathbf{h} is a history vector, h is the thickness of the disc, and r_1 and r_2 are the radii of the two nodes respectively. The element right-hand side vector can be written as:

$$\mathbf{R}^e = \int_V (\mathbf{N}^T \mathbf{f} - \mathbf{B}^T \mathbf{h}) dV = 2\pi \int_{-h/2}^{h/2} \int_{r_1}^{r_2} (\mathbf{N}^T \mathbf{f} - \mathbf{B}^T \mathbf{h}) r dr dz$$

where \mathbf{N} is the shape function vector, \mathbf{f} is the body force vector.

Birefringence Prediction

Flow induced birefringence is caused by the shear induced molecular orientation developed during the filling and packing stages, and can be frozen in the solidified layers during the cooling of the polymer melt. The following nonlinear viscoelastic constitutive equation is employed for the modeling of the flow induced stress [4, 5]:

$$\boldsymbol{\sigma} = -P(\rho, T) \mathbf{I} + \int_{-\infty}^t M(\xi(t) - \xi(\tau)) h(I_1, I_2) \mathbf{C}_r^{-1}(\tau) d\tau \quad (7)$$

where $M(\xi(t) - \xi(\tau))$ is the memory function defined as:

$$M(\xi(t) - \xi(\tau)) = -\frac{dG(\xi(t) - \xi(\tau))}{dt} = \sum_{i=1}^m \frac{g_i}{a_T \theta_i} e^{-\frac{\xi(t) - \xi(\tau)}{\theta_i}}$$

where $G(\xi(t))$ is the relaxation modulus, $h(I_1, I_2)$ is the damping function, $\mathbf{C}_r^{-1}(\tau)$ is the Finger strain tensor, and I_1 , I_2 , and I_3 are its three invariants. The damping function proposed by Wagner et al [4] is adopted in the current study:

$$h(I_1, I_2) = m^* \exp(-n_1 \sqrt{I-3}) + (1-m^*) \exp(-n_2 \sqrt{I-3})$$

where m^* , n_1 , n_2 are material dependent coefficients. Applying the empirical Cox-Merz rule [6], these coefficients are obtained by fitting the complex viscosity from dynamic mechanical test with the following equation:

$$\eta = \sum_{i=1}^m \left[m^* \frac{\eta_i \theta_i^2}{(1 + n_1 \theta_i \dot{\gamma})^2} + (1 - m^*) \frac{\eta_i \theta_i^2}{(1 + n_2 \theta_i \dot{\gamma})^2} \right] \quad (8)$$

A modified stress-optical rule [7] is applied to calculate the birefringence once the flow induced stress and normal stress differences are obtained:

$$n_r^d = \int_{-\infty}^t C_{t-\tau} \sigma_\tau^d d\tau \quad (9)$$

where C is a temperature dependent coefficient which is characterized by dynamic stress-optical measurement, n^d is the birefringence, σ^d is the deviatoric stress, and τ is time. The time-temperature superposition holds for the stress-optical coefficient.

The thermally induced birefringence is caused by the thermal stress in the molded parts, which results from the rapid cooling process coupled with the viscoelastic properties of the polymer. The thermally induced vertical birefringence is calculated by:

$$\Delta n_{rz} = n_r - n_z = \int_{-\infty}^{t_g} C_{t-\tau} \frac{d\Delta\sigma}{d\tau} d\tau + C_g (\sigma_r - \sigma_z) \quad (10)$$

where σ_r and σ_θ are the residual radial and hoop stresses in the part, and t_g is the time when the temperature polymer at that material point just falls below T_g . The thermally induced in-plane birefringence arises only from the stress difference caused by the warpage of the disc due to asymmetric cooling. The classic stress-optical rule is applied to calculate the in-plane cooling birefringence in the glassy state:

$$\Delta n_{r\theta} = n_r - n_\theta = C_g (\sigma_r - \sigma_\theta) \quad (11)$$

Results and Discussion

The effects of mold and melt temperatures on mold displacement, warpage, and birefringence are studied. Unless otherwise specified, each condition under investigation is varied as low, median and high values with other processing conditions set to the median values. The low, median, high mold and melt temperatures are 100°C, 107°C, 114°C, and 300°C, 310°C, 320°C respectively. The initial mold cavity thickness is set to be 1.15 mm before molding. The experimental and simulated mold displacement curves under different mold and melt temperatures are shown in Fig. 1 and Fig. 2 respectively. As is shown by the figures, the general magnitude of the simulated mold displacement compares with the experiments.

With respect to birefringence, the experimental and simulated path differences as a function of radius for mold temperatures of 100°C and 114°C with melt temperatures of 300°C and 320°C are shown in Fig. 3. The path difference of the incident laser beam Γ_z is a direct measurement of the

in-plane birefringence, and is the integration of the in-plane birefringence over the thickness of the disc:

$$\Gamma_z = \int_{-h/2}^{h/2} (n_r - n_\theta)_z dz \quad (12)$$

As the mold or mold temperature increases, the in-plane birefringence decreases significantly due to increased stress relaxation at higher temperature.

The experimental and simulated warpage under low and high mold and melt temperatures are shown in Fig. 5 and Fig. 6 respectively, with the warpage under median temperatures shown in Fig. 4. It can be seen from the figures that compared with melt temperature, mold temperature has a much greater effect on warpage. It is also interesting to note that gravity play a significant role in the warpage development. As shown in Fig. 7 for the warpage of a DOE run, the result from the simulation including the gravity effect is much closer to the experimental data.

Conclusions

The hybrid finite element/finite difference method originated by Chiang et al [1] to solve the temperature and pressure fields of a non-isothermal compressible flow for the simulation of injection molding is extensible to injection-compression molding. While the mold and melt temperature have similar effects on birefringence, the mold temperature has a much greater effect on the magnitude of warpage. For the optical grade polycarbonate considered, the thermally induced birefringence caused by the warpage of the disc is significant, the neglect of which will cause significant prediction errors. Since warpage in injection and injection-compression molded parts is almost always present, much attention should be paid to the influence of the warpage when performing simulation and validation of birefringence.

With an improved understanding of the process and quality dynamics, it is possible to produce optical media with greater data density and bonded layers.

References

- [1] Chiang, H.H., C.A. Hieber, and K.K. Wang, *Polymer Engineering and Science*. **31** (2) 116-124 (1991)
- [2] Baaijens, F.P.T., *Rheologica Acta*. **30** 284-299 (1991)
- [3] Rockey, K.C., H.R. Evans, and D.W. Griffiths, The Finite Element Method. 2nd ed. John Wiley & Sons. New York (1983)
- [4] Wagner, M.H., *Rheologica Acta*. **15** 136-142 (1976)
- [5] Wagner, M.H., *Rheologica Acta*. **16** 43-50 (1977)
- [6] Cox, W.P. and E.H. Merz, *Journal of Polymer Science*. **28** 619-622 (1958)
- [7] Wimberger-Friedl, R. and J.G.D. Bruin, *Rheologica Acta*. **30** 419-429 (1991)

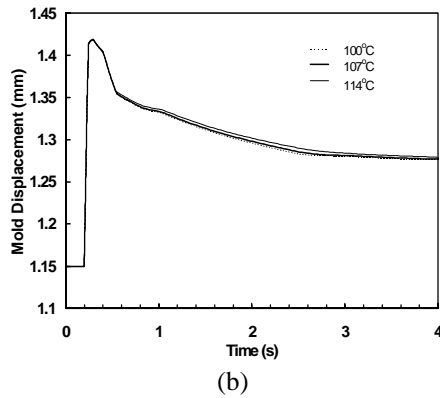
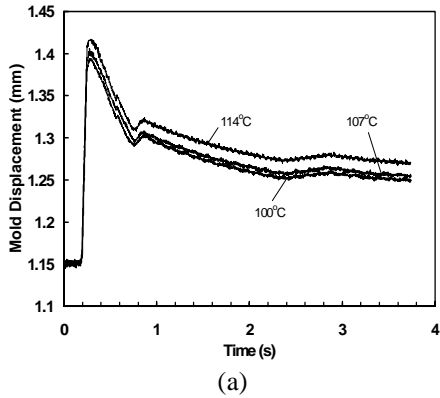


Fig. 1 Mold displacement at different mold temperatures: (a) experiment (b) simulation.

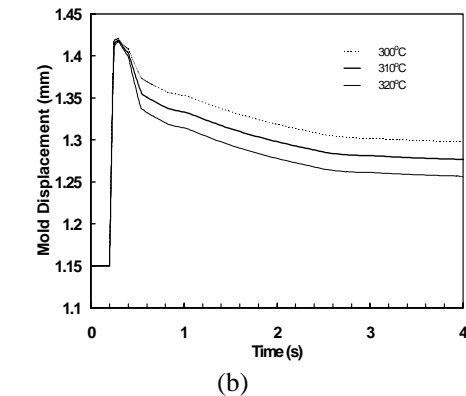
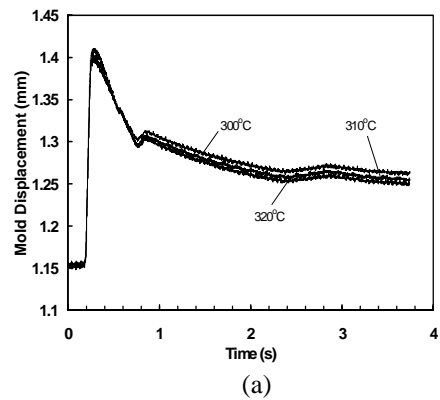


Fig. 2 Mold displacement at different melt temperatures: (a) experiment (b) simulation

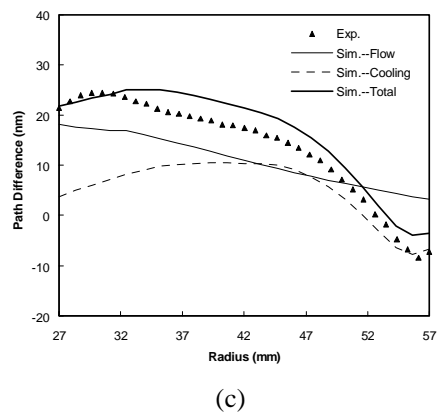
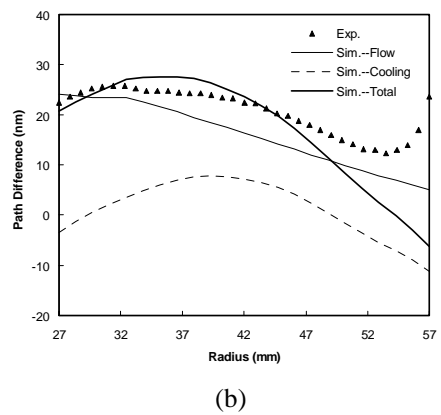
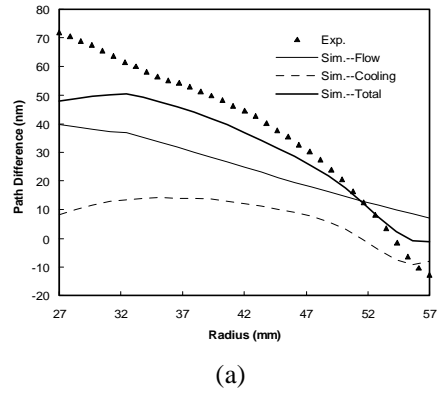


Fig. 3 Path difference as a function of radial location: experiment vs. simulation. (a) $T_{melt}=300^{\circ}\text{C}$ and $T_{mold}=100^{\circ}\text{C}$. (b) Same as (a) except for $T_{mold}=114^{\circ}\text{C}$. (c) Same as (a) except for $T_{melt}=320^{\circ}\text{C}$.

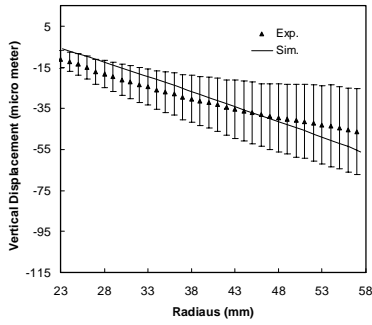
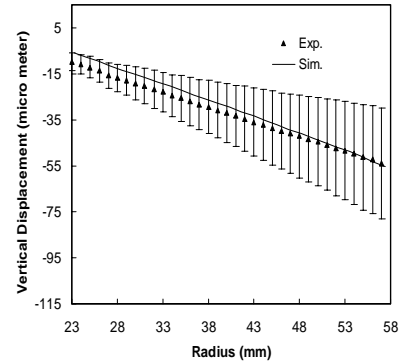
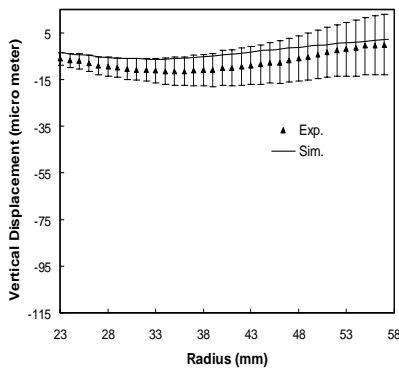


Fig. 4 Warpage of a disc under median processing condition. The error bars are the 95% confidence intervals for the measured warpage.



(a)



(a)

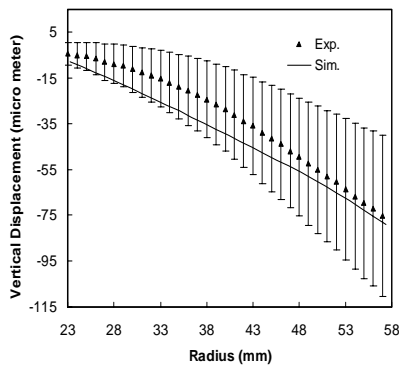


Fig. 5 Warpage of discs at different mold temperatures: (a) $T_{\text{mold}}=100^{\circ}\text{C}$ (b) $T_{\text{mold}}=114^{\circ}\text{C}$. The error bars are the 95% confidence intervals of the measured warpage.

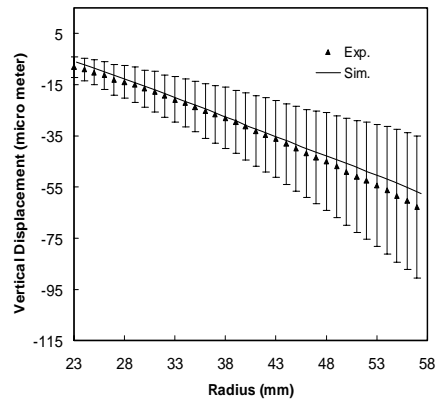


Fig. 6 Warpage of discs at different melt temperatures: (a) $T_{\text{melt}}=300^{\circ}\text{C}$ (b) $T_{\text{melt}}=320^{\circ}\text{C}$. The error bars are the 95% confidence intervals of the measured warpage.

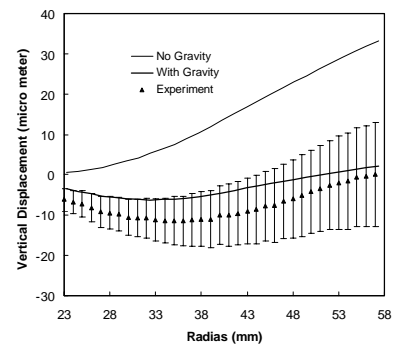


Fig. 7 Comparison of measured warpage and simulated warpage with and without gravity effect.